2466 *Chem. Mater.* **2010,** *22,* 2466–2473
DOI:10.1021/cm902883p

CHEMISTRY OF MATERIALS
Article

Formation and Growth Mechanisms of Imogolite-Like Aluminogermanate Nanotubes

C. Levard,[†] J. Rose,*[,†] A. Thill,[§] A. Masion,[†] E. Doelsch,[‡] P. Maillet,[§] O. Spalla,[§] L. Olivi,[⊥] A. Cognigni,[⊥] F. Ziarelli,[▽] and J.-Y. Bottero[†]

[†]*CEREGE, Aix-Marseille University, CNRS, IRD, Collège de France, Europôle Méditerranéen de L'Arbois, BP 80, 13545 Aix en Provence, France,* [‡]*CIRAD, Environmental Risks of Recycling Research Unit, 34398 Montpellier, France,* [§]*CEA Saclay, IRAMIS, Laboratoire Interdisciplinaire sur l'Organisation Nanométrique et Supramoléculaire, 91191 Gif sur Yvette, France,* [⊥]*ELETTRA, Synchrotron Light Source, 34012 Trieste, Italy, and* [▽]*Spectropole, Fédération des Sciences Chimiques CNRS-FR1739, av. Escadrille Normandie Niémen, 13397 Marseille cedex 20, France*

Received September 15, 2009. Revised Manuscript Received January 12, 2010

The growth mechanisms of imogolite-like aluminogermanate nanotubes have been examined at various stages of their formation. The accurate determination of the nucleation stage was examined using a combination of local- (XAS at the Ge−K edge and ^{27}Al NMR) and semilocal scale technique (in situ SAXS). For the first time, a model is proposed for the precursors of the nanotubular structure and consist in rooftile-shaped particles, up to 5 nm in size, with ca. 26% of Ge vacancies and varying curvatures. These precursors assemble to form short nanotubes/nanorings observed during the aging process. The final products are most probably obtained by an edge−edge assembly of these short nanotube segments.

Introduction

Over the past two decades, there has been an increasing interest in non-carbon-based nanotubes, because of their unique properties, in terms of chemical reactivity, optical properties, and a high specific surface area. The literature generally considers that the first synthesis of an inorganic nanotube (tungsten disulfide) was performed in 1992 by Tenne et al.[1−3] Since this date, numerous protocols to obtain other inorganic nanotubes have been developed, including template processes,[4,5] reverse micellar systems,[6] vapor depositions,[7] and electrochemical reactions.[8] Nevertheless, imogolite ($Al_2SiO_7H_4$) nanotubes were successfully synthesized even sooner, in 1977.[9] Imogolite is a natural mineral formed in volcanic soils. It consists of a single-walled aluminosilicate nanotube with inner and outer diameters of 1 and 2 nm, respectively, and a length ranging from a few tens to several hundreds of nanometers. The wall of the imogolite nanotube is composed of a curved gibbsite ($Al(OH)_3$) layer on the outer surface and silicate tetrahedra linked to six aluminum octahedra inside the tube.[10] It was observed in natural systems for the first time in 1962,[11] and its structure was well-characterized 10 years later using X-ray diffraction (XRD).[10] The synthesis of imogolite nanotubes involves a simple hydrolysis step followed by a growth step at 95 °C.[9,12] This very simple synthesis protocol is in contrast to the far-more-complicated multiple-step processes generally implemented in nanofabrication and, thus, explains the great interest for imogolite nanotubes.

However, almost all current imogolite synthesis protocols are not suited to readily yield significant amounts of material. Indeed, since the initial concentration of reagents lies in the millimolar range,[9] the synthesis of only 1 g of imogolite involves processing an initial reaction volume of at least 10 L. In a recent study, larger nanotube amounts could be obtained, but at the cost of a considerably longer growth step.[13] Such drawbacks hinder the transition from the laboratory scale to the pilot/industrial scales, thereby diminishing the interest in the development of the applications for imogolite nanotubes. Efforts to control and improve reaction yield, length, and diameter of the nanotubes requires the knowledge of the growth mechanisms of the nanotubes, i.e., identifying the

*Author to whom correspondence should be addressed. Tel.: (+33) 442 97 15 29. E-mail: rose@cerege.fr.

(1) Tenne, R.; Margulis, L.; Genut, M.; Hodes, G. *Nature* **1992**, *360*, 444.
(2) Remskar, M. *Adv. Mater.* **2004**, *16*(17), 1497.
(3) Tenne, R. *Nature Nanotechnol.* **2006**, *1*, 103.
(4) Mayya, K. S.; Gittins, D. I.; Dibaj, A. M.; Caruso, F. *Nano Lett.* **2001**, *1*(12), 727.
(5) Wang, C. C.; Kei, C. C.; Yu, Y. W.; Perng, T. P. *Nano Lett.* **2007**, *7*, 1566.
(6) Lisiecki, I.; Sack-Kongehl, H.; Weiss, K.; Urban, J.; Pileni, M. P. *Langmuir* **2000**, *16*(23), 8802.
(7) Liu, Z. W.; Bando, Y. *Adv. Mater.* **2003**, *15*(4), 303.
(8) Zhao, A. W.; Meng, G. W.; Zhang, L. D.; Gao, T.; Sun, S. H.; Pang, Y. T. *Appl. Phys. A* **2003**, *76*(4), 537.
(9) Farmer, V. C.; Fraser, A. R.; Tait, J. M. *J. Chem. Soc., Chem. Commun.* **1977**, 462.
(10) Cradwick, P. D. G.; Farmer, V. C.; Russel, J. D.; Masson, C. R.; Wada, K.; Yoshinaga, N. *Nat. Phys. Sci.* **1972**, *240*, 187.
(11) Yoshinaga, N.; Aomine, S. *Soil Sci. Plant Nutr.* **1962**, *8*(3), 22.
(12) Yang, H.; Wang, C.; Su, Z. *Chem. Mater.* **2008**, *20*(13), 4484.
(13) Levard, C.; Masion, A.; Rose, J.; Doelsch, E.; Borschneck, D.; Dominici, C.; Ziarelli, F.; Bottero, J.-Y. *J. Am. Chem. Soc.* **2009**, *131*, 17080.

 Published on Web 03/25/2010

nature and structure of precursor structure and how they assemble into a nanotubular structure. The accurate determination of the nucleation stage requires in situ characterization by combining local-scale and semilocal-scale techniques, such as X-ray absorption spectroscopy (XAS), nuclear magnetic resonance (NMR), and small-angle X-ray scattering (SAXS). However, a detailed determination of the growth mechanism could not be obtained to date, because of limitations specific to each technique. Because of the low difference in electronic contrast between Al and Si, XAS is not well-suited to determine the coordination environment of these two elements. The use of in situ SAXS to study the semilocal scale (size and shape) is generally limited, because of the low concentration of nanotubes in solution and a relatively low electronic contrast with the solvent, both leading to a poor signal/noise ratio. NMR has proven to be useful to characterize the final synthesis products; however, until now, no description of the imogolite formation based on NMR data is available in the literature.

One way to overcome these difficulties in gaining new insights in the formation mechanisms of imogolite-type nanotubes is to use an aluminogermanate analogue of imogolite (Ge-imogolite). Indeed, several authors reported the synthesis of imogolite-like nanotubes ($Al_2GeO_7H_4$) by substituting silicon with germanium.[14−19] These nanotubes exhibit a higher electronic contrast, thus enhancing XAS and SAXS sensitivity. A recent study investigating the growth mechanisms of Ge-imogolite nanotubes revealed that the Ge-imogolite formation is the result of the recombination of amorphous nanoscale nuclei of ~6 nm.[18] However, the structure and composition of these precursors could not be determined, because the low amount of materials prevented the authors from using in situ SAXS. Moreover, no XAS was used to determine the evolution of a Ge atomic environment during the growth stage.

Recently, a new synthesis protocol allowed the formation of the aluminogermanate nanotubes from solutions 100 times more concentrated than previously reported protocols,[16] thus opening the route for an in situ SAXS characterization of the formation mechanisms of the aluminogermanate nanotubes. Therefore, the obtained Ge-imogolite is, of course, structurally identical to the natural aluminosilicate, with the only differences being the expected larger (and almost monodisperse) tube diameter, because of Ge and a shortened tube length.

The objective of the present study is to take advantage of the improved analysis conditions enabled by this new synthesis protocol, in terms of electron contrast and concentration, to further investigate the growth mechanisms of Ge-imogolite. To this end, samples obtained at different stages of the synthesis were examined by a combination of local-scale (XAS at the Ge−K edge and ^{27}Al NMR) and semilocal-scale techniques (SAXS).

Materials and Methods

Synthesis of the Aluminogermanate Nanotubes. Tetraethoxygermanium was added to a 0.5 mol L^{-1} aluminum perchlorate solution. The [Al]/[Ge] ratio was set to 2. The mixture was then slowly hydrolyzed by addition of a NaOH solution (0.5 mol L^{-1} at 1.5 mL min^{-1}) until a hydrolysis ratio ([OH]/[Al]) of 2 was reached. This ratio corresponded to a pH value of 3.5. The aluminum concentration after base addition was 0.167 mol L^{-1}. The obtained solution was stirred during 12 h. At this point, a third of the solution was set aside for the structural study of the precursor ($t = 0$ days). The remainder solution was divided to obtain samples heated at 95 °C in Teflon bottles for 2 and 5 days. For each of the three samples, half were dialyzed using a 8000 Da membrane against ultrapure water (dialysate/retentate volume ratio = 100), to withdraw residual salts and excess alcohol. Thus, six samples were obtained: three dialyzed and three nondialyzed solutions at $t = 0$, 2, and 5 days. SAXS measurements were performed in situ, i.e., on the nondialyzed suspensions, whereas freeze-dried samples were used for NMR and XAS characterization.

Structural Characterization. *EXAFS.* Extended X-ray absorption fine structure spectroscopy (EXAFS) spectra were recorded in transmission mode on beamline 11.1 at the ELETTRA synchrotron (Trieste, Italy). Spectra were acquired using a Si(111) monochromator above the Ge K-edge (11 103 eV). The ion chambers for incident and transmitted beam were filled with argon and nitrogen gas. The high signal/noise ratio permitted EXAFS spectra to be scanned up to 16 $Å^{-1}$. EXAFS spectra were analyzed using standard procedures for data reduction with a set of software developed by Michalowicz.[20] EXAFS oscillations were recalculated using amplitude and phase functions obtained with the FEFF8 code.[21,22] FEFF functions were validated for each scattering path by modeling the spectra of well-characterized crystalline model compounds (Ge oxide and Ge-talc). The uncertainties on R (distance between two atoms) and N (number of atoms) were ±0.01 Å and ±10%, respectively.[23]

NMR. ^{27}Al single-pulse magic-angle spinning (SP MAS) NMR spectra were obtained with a Bruker Avance 400 MHz WB spectrometer (magnetic field 9.4T) operating at a ^{27}Al resonance frequency of 104.3 MHz and using a commercial Bruker 2.5 mm double-bearing probe head. Approximately 12 mg of samples were placed in a zirconium dioxide rotor with an outer diameter of 2.5 mm and

(14) Ackerman, W. C.; Smith, D. M.; Huling, J. C.; Kim, Y. W.; Bailey, J. K.; Brinker, C. J. *Langmuir* **1993**, *9*(4), 1051.
(15) Konduri, S.; Mukherjee, S.; Nair, S. *ACS Nano* **2007**, *1*(5), 393.
(16) Levard, C.; Rose, J.; Masion, A.; Doelsch, E.; Borschneck, D.; Olivi, L.; Dominici, C.; Grauby, O.; Woicik, J. C.; Bottero, J.-Y. *J. Am. Chem. Soc.* **2008**, *130*(18), 5862.
(17) Mukherjee, S.; Bartlow, V. M.; Nair, S. *Chem. Mater.* **2005**, *17*, 4900.
(18) Mukherjee, S.; Kim, K.; Nair, S. *J. Am. Chem. Soc.* **2007**, *129*(21), 6820.
(19) Wada, S.-I.; Wada, K. *Clays Clay Miner.* **1982**, *30*(2), 123.
(20) Michalowicz, A. *J. Phys. IV* **1997**, *7*(C2), 235.
(21) Ankudinov, A. L.; Bouldin, C. E.; Rehr, J. J.; Sims, J.; Hung, H. *Phys. Rev. B* **2002**, *65*(10), 104107.
(22) Newville, M. *J. Synchrotron Radiat.* **2001**, *8*, 96.
(23) Teo, B. K. *EXAFS: Basic Principle and Data Analysis*; Springer−Verlag: Berlin, Heidelberg, New York, Tokyo, 1986; p 349.

Table 1. ICP−AES Analysis of Al and Ge Quantities in the Dialysate and Retentate for Samples at t = 0, 2, and 5 Days of Aging[a]

		Value at Time t		
		t = 0 day	t = 2 days	t = 5 days
total Ge and Al quantity In the solution (mol)	Ge	1.46×10^{-3}	1.46×10^{-3}	1.46×10^{-3}
	Al	3.33×10^{-3}	3.33×10^{-3}	3.33×10^{-3}
(=A)	Al/Ge	2.28	2.28	2.28
Ge and Al quantity in the dialysate (mol) (= B)	Ge	0.94×10^{-3}	0.24×10^{-3}	0.29×10^{-3}
	Al	2.24×10^{-3}	1.03×10^{-3}	1.06×10^{-3}
total Ge and Al quantity in the retentate (mol) (calculated from A−B)	Ge (= C)	0.52×10^{-3}	1.22×10^{-3}	1.17×10^{-3}
	Al (= D)	1.09×10^{-3}	2.30×10^{-3}	2.27×10^{-3}
Al/Ge ratio in the dialyzed solid sample	calculated (from D/C)	2.10	1.89	1.94
	measured (ICP)	2.14	1.93	1.95

[a] Quantities are given in absolute values, to simplify the mass balance determination.

spun at a magic-angle spinning rate of 20 kHz. Typical acquisition parameters included 1.0 μs 90° pulse, 2 s recycle delays, 528 scans and an acquisition time of 20 ms. Chemical shifts were referenced to 1 M $Al(NO_3)_3$ solution, whose resonance was set to 0 ppm.

SAXS. The experimental setup includes a rotating anode and collimating optics that provide a monochromatic beam ($\lambda = 0.1548$ nm) with a 1 mm × 1 mm raster at the sample position with a total incident flux of 10^7 photons/s. The transmitted flux is measured by an ionization chamber after the sample. A gas detector is placed after the 300-mm-diameter output window of the vacuum chamber at a distance of 1180 mm from the sample. The direct beam hits an opaque lead beamstop in a position as asymmetric as possible, to increase the range of scattering vectors. In this configuration, a ratio of q_{max}/q_{min} of 34 is reached with $q_{max} = 0.5$ Å^{-1} and $q_{min} = 0.015$ Å^{-1}. The scattering vector (q) is defined as $q = k_d - k_i$ (the wave vectors of the incident and diffracted beams) and has a modulus of $q = 4\pi \sin(\theta)/\lambda$, where λ is the incident wavelength and 2θ is the scattering angle. The counting time is 1800 s, and the signal is corrected for background. Standard procedures are applied to obtain the scattered intensity in units of cm^{-1}, as a function of the scattering vector q.[24]

Atomic models of nanotubes and nanotube precursors were constructed using a locally developed computer code. The code applies symmetry relationships to built imogolite of various sizes and curvature. The average scattering intensity ($I_m(q)$) of a single atomic model, expressed in units of cm^2, is obtained using the Debye formula (eq 1):

$$I_m(q) = \sum_i \sum_j f_i f_j \frac{\sin(qr_{ij})}{qr_{ij}} \quad (1)$$

where r_{ij} is the distance between the ith and jth atoms, and f_i and f_j are the atomic scattering factors of the ith and jth atoms. At a low scattering vector, f_i and f_j are approximated to be the average excess electron number of the atoms (taking into account an average solvent electronic density of 0.33 e$^-$/Å^3) multiplied by the Thomson scattering length (0.284×10^{-12} cm).

The comparison with the experimental intensity (expressed in units of cm^{-1}) is obtained by multiplying $I_m(q)$ (expressed in units of cm^2) with the concentration of nanoparticles in cm^{-3}).

Results

Dialysis Experiment and Quantification of the Nonreactive Phase. The [Al]/[Ge] ratio before hydrolysis was quantified by ICP-AES and found equal to 2.28. The discrepancy between the theoretical ([Al]/[Ge] = 2) and experimental value may arise from the low stability of tetraethoxygermanium. Fast hydration and/or drying of the reagent may be responsible for the missing germanium fraction (precipitation/adsorption at the surface of sampling devices).

The quantification of the Ge and Al in the dialysate at t = 0 days (see Table 1) indicated that 64% of Ge and 67% of Al are either unreacted (monomers) or involved in species (oligomers) small enough to cross the 8000 Da dialysis membrane. Nanotube precursors, which are assumed to be in the retentate, represent only a small fraction of the initial amount of atomic Al and Ge. After two days of heating, the proportions of Ge and Al in the dialysate decreased to 16% and 31%, respectively, and did not evolve significantly upon further heating.

Structural Local Scale Characterization. For all three dialyzed samples at t = 0, 2, and 5 days, the ^{27}Al MAS NMR spectra display a single downfield resonance at 6.8 ± 0.1 ppm (see Figure 1, top), which is in the chemical shift region indicative of 6-fold O-coordinated Al.[25,26] This shift is within the 5−7 ppm range reported for Si-imogolite[27] and is a slightly lower than the 8−11 ppm shift range reported for Al in gibbsite.[25,28] Therefore, this 6.8 ppm line can be attributed to Al in larger clusters with

(24) Narayanan, T. Synchrotron Small-Angle X-Ray Scattering. In *Soft Matter: Scattering, Imaging and Manipulation*; Borsali, R.; Pecora, R., Eds.; Springer: Berlin/Heidelberg, 2008; Vol. III, pp 1−59.

(25) Kinsey, R. A.; Kirkpatrick, R. J.; Hower, J.; Smith, K. A.; Oldfield, E. *Am. Mineral.* **1985**, *70*(5−6), 537.

(26) Akitt, J. W. *Multinuclear Studies of Aluminium Compounds*; Elsevier Science: Oxford, U.K., 1989; Vol. *21*, p 149.

(27) Goodman, B. A.; Russell, J. D.; Montez, B.; Eric, O.; Kirkpatrick, R. J. *Phys. Chem. Miner.* **1985**, *12*(6), 342.

(28) Smith, M. E. *Appl. Magn. Reson.* **1993**, *4*, 1–64.

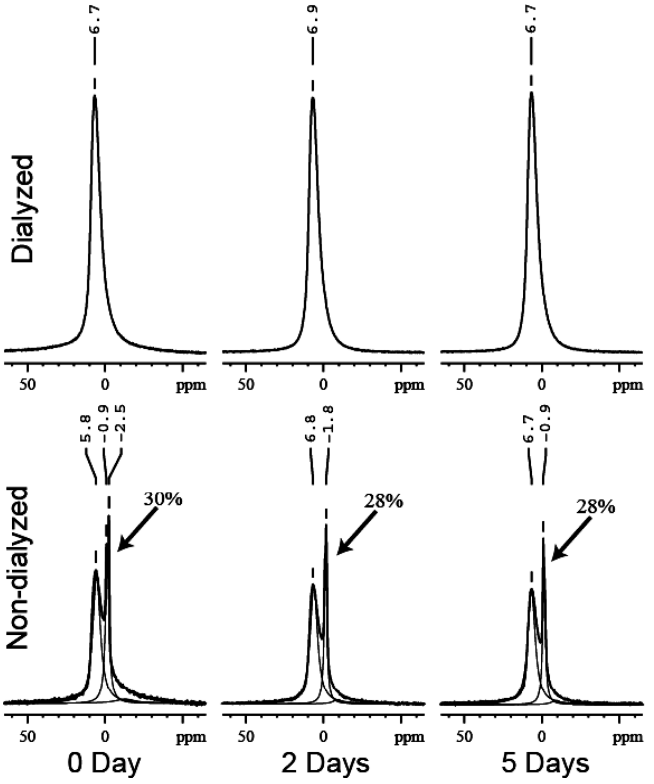

Figure 1. ^{27}Al NMR spectra of (top) dialyzed samples and (bottom) nondialyzed samples and proportion of monomeric Al obtained by line-fitting after t = 0, 2, and 5 days of aging.

a gibbsite structure, with the lower chemical shift than the "infinite" gibbsite phase being a consequence of a lesser polymerization level.[29] Tetrahedrally coordinated aluminum was not detected in our samples, as opposed to previous observations, revealing various amounts of 4-fold coordinated Al with a shift of ~55−60 ppm in products obtained using the same synthesis protocol, with Si instead of Ge.[27]

The NMR spectra of the nondialyzed samples (Figure 1, bottom) also show a contribution in the 5−7 ppm range and is attributed to the same local environment of Al. In the case of the nondialyzed samples, there is a difference between $t = 0$ and more-aged samples: at $t = 0$, the 5.8 ppm chemical shift could be either due to a lesser polymerization level of Al, or be the consequence of overlapping resonances. Upon heating of the material, the chemical shift at 6.7 ppm for this line is identical to the dialyzed samples. Besides a signal in the 5−7 ppm range, the spectra of the three nondialyzed samples (Figure 1, bottom) display additional sharp resonances of ~0 ppm and −2 ppm, corresponding to unreacted Al monomers. Indeed, the 0-ppm shift corresponds to the reference $Al(H_20)_6$ octahedron and the −2 ppm line is identical to the shift observed for the solid Al perchlorate. The amount of nonreactive monomeric Al can be estimated by peak surface integration (see Figure 1, bottom). The proportion of unreacted monomers obtained by peak surface integration is ~30% of the initial Al for all three samples.

The $k^3(\chi(k))$ EXAFS spectra and radial distribution functions (Figure 2) of the six samples are very similar. Indeed, all spectra could be fitted with the same two atomic contributions, i.e., O atoms in the first coordination shell and Al atoms on the second one. The fitting parameters are summarized in Table 2. For all six samples, the first shell is characteristic of a tetrahedral coordination of Ge atoms as observed for Ge-imogolite.[16] As expected, at all reaction times, the number of Al atoms in the second coordination sphere of Ge is lower for the nondialyzed than for the dialyzed sample (Table 2). This difference is less pronounced from t = 2 days. For the dialyzed samples, the number of Al atoms in the second shell increases from 4.5 ± 10% at $t = 0$ days to ~6 ± 10% for t = 2 and 5 days (see Table 2). This Ge coordination after 2 and 5 days is consistent with the local environment of Ge described for imogolite.[16] Since the EXAFS signal corresponds to an average over the entire sample, the lower number of detected Al atoms for $t = 0$ days may be the result of the presence of multiple binding environments for Ge.

Structural Characterization at the Semilocal Scale. The structure at a larger scale was examined by SAXS for the same samples as above, i.e., at $t = 0$, 1, 2, 3, and 5 days (see Figure 3). The sample at t = 0 days shows a scattering signal, which confirms the presence of a condensed phase. The scattered intensity levels off at $q < 0.08-0.1$ Å^{-1}, indicating a maximum particle size of ~4−5 nm, which is in the same size range than the 6-nm precursors reported from previous light scattering results.[18] Upon heating, the scattering signal displays oscillating intensities for $q >$ 0.1 Å^{-1}. These oscillations already become visible at $t =$ 1 day. As the reaction time increases, the oscillations are not shifted in q but are more pronounced for the samples at $t = 2$ and 3 days. The samples at $t = 3$ and 5 days have quasi-identical scattering curves. The intensity maximum at low q increases sharply from $t = 0$ days to $t = 3$ days and is constant thereafter. The last curve (for t = 5 days) corresponds to a suspension of nanotubes with a mean diameter of 3 nm and length of ~20 nm.[16] It can be reasonably assumed that the lower small-angle intensity maximum for $t = 1$ and 2 days is due to shorter nanotubes with the same diameter and possibly remaining precursors.

This is one general property of scattering where the second momentum of the intensity (called the "invariant", Q) is not dependent on the structure of the scattering sample but only on the volume fraction and scattering length density contrast ($\Delta\rho$) of the scattering objects:[30]

$$Q = \int_0^\infty I(q)q^2 \, dq = 2\pi^2(\Delta\rho)^2 V$$

When Q is computed in the experimental q range of 0.015−0.45 Å^{-1}, the ratio Q/Q_0 (where Q_0 is the invariant

(29) Kirkpatrick, R. J.; Smith, K. A.; Schramm, S.; Turner, G.; Yang, W.-H. J. *Ann. Rev. Earth Planet. Sci.* **1985**, *13*, 29.

(30) Glatter, O.; Kratky, O. *Small Angle X-ray Scattering*; Academic Press: London, 1982; p 525.

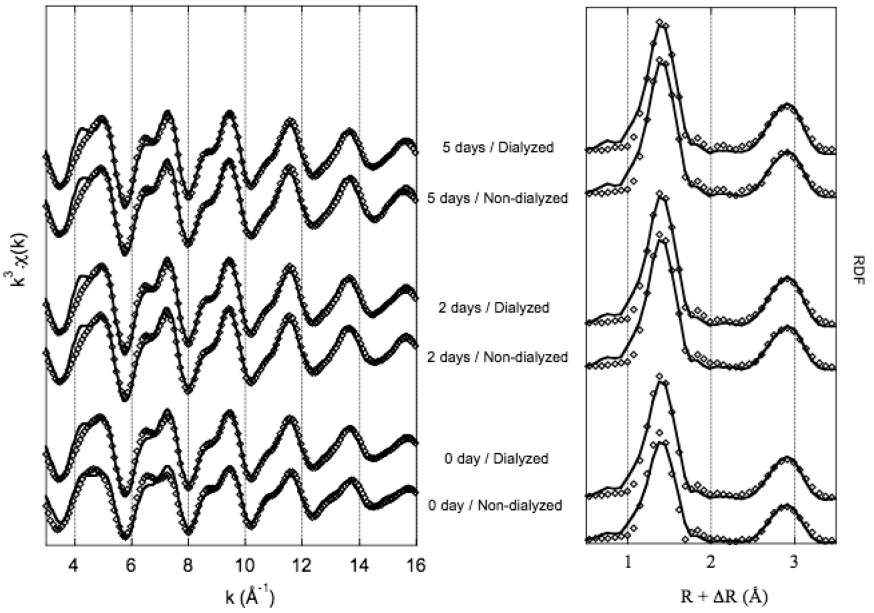

Figure 2. Plots showing $k^3(\chi((k))$ EXAFS spectra and radial distribution functions (RDFs) at the Ge−K edge of dialyzed and nondialyzed samples after 0, 2, and 5 days of aging.

Table 2. Ge K-Edge EXAFS Fitting Parameters of the Calculated Spectra

		Ge−O Shell			Ge−Al Shell		
samples	*R* window (Å)	coordination number, N_O[a]	radial distance, R[b]	Debye−Waller factor, σ (Å)	coordination number, N_{Al}	radial distance, *R*	Debye−Waller factor, σ (Å)
t = 0 days							
dialyzed	1.07−3.34	4.2	1.75	0.05	4.5	3.26	0.07
nondialyzed	1.07−3.36	3.8	1.71	0.06	3.4	3.26	0.07
t = 2 days							
dialyzed	1.07−3.36	4.5	1.75	0.05	5.5	3.26	0.08
nondialyzed	1.07−3.36	4.4	1.75	0.05	4.9	3.26	0.08
t = 5 days							
dialyzed	1.07−3.47	4.4	1.75	0.05	5.9	3.26	0.08
nondialyzed	1.07−3.36	4.4	1.75	0.05	5.3	3.26	0.08

[a] Standard deviation of ±10%. [b] Standard deviation of ±0.02 Å.

for the sample at $t = 0$) is 1.08 and 0.96 for $t = 2$ and 5 days, respectively. Thus, there is no significant variation of the volume fraction of scattering objects between the samples. This suggests that the nanotubes grow from smaller particles with almost the same electronic density as the nanotube wall.

Discussion

Unreacted Phase and Precursor Proportion. The dialysis allows excess salts, as well as unreacted Al and Ge, to be removed from the sample (the retentate). NMR results indicate that, at all reaction times, the proportion of Al monomers (Al_m) in the nondialyzed sample is ~30% of the initially introduced Al (i.e., $Al_m = 3.33 \times 10^{-3} \times 30\% = 0.99 \times 10^{-3}$ mol). For the systems at $t = 2$ and 5 days, this monomeric Al fraction accounts for almost all of the Al measured by ICP-AES in the dialysate, viz, 1.03×10^{-3} mol and 1.06×10^{-3} mol for $t = 2$ and $t = 5$ days, respectively (see Table 1).

For the sample at $t = 0$ days, however, the quantities of Al and Ge measured in the dialysate are significantly higher ($Al = 2.24 \times 10^{-3}$ mol) than those for $t = 2$ and 5 days. According to our NMR data, only 45% of this amount corresponds to Al monomers. The remaining

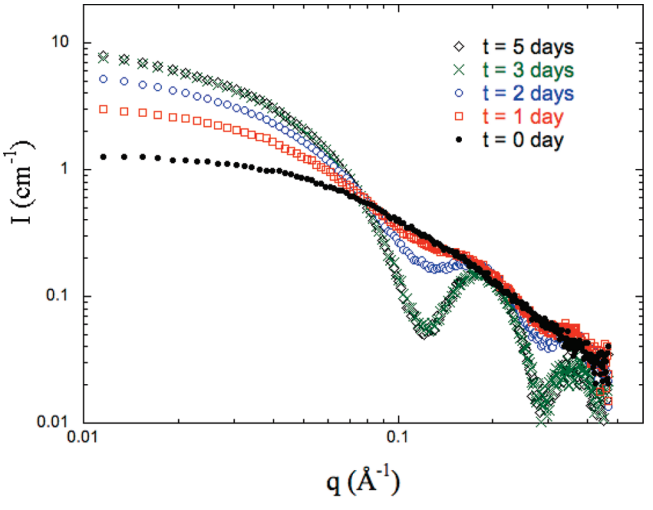

Figure 3. Small-angle X-ray scattering (SAXS) intensities measured at t = 0, 1, 2, 3, and 5 days of aging.

fraction of Al in the dialysate consists of small Al polymers, also called oligomers, whose sizes are smaller than the pore size of the dialysis membrane. There is no well-defined resonance associated with this high proportion of oligomers (about one-third of the initial Al) on the NMR spectrum. Al oligomers, or generally speaking, poorly polymerized Al species typically have a resonance in the 3−6 ppm range.[26,31] The 5.8 ppm peak may then be due to the overlap of the 6.7 ppm peak corresponding to the retentate (Figure 1) with Al_o resonance(s) rather than to a single Al coordination environment.

Precursor Structure. At $t = 0$ days, Al and Ge are present in the form of monomers and oligomers, which can be dialyzed, and larger polymers that remain in the retentate. (Hereafter, this polymeric fraction will be called "precursor".) The atomic environment of Al and Ge in the precursors exhibit substantial differences, compared to fully formed Ge-imogolite nanotubes.

Indeed, for the dialyzed sample (i.e., the polymeric fraction) at $t = 0$, the Ge K-edge EXAFS data are fitted using the same Ge−O and Ge−Al distances as in the fully developed imogolite structures but with a much lower number of Al atoms around Ge tetrahedra ($N = 4.5 \pm 10\%$, instead of 6). Considering a fully developed imogolite, the effect of tube length on the number of neighboring Al atoms around Ge can be calculated. The GeO_4 tetrahedra sites are either in the core of the tube (Ge_{co}), where 6 Al atoms surround Ge, or at the end of the tube ("edge sites" Ge_{es}), where an average of 3 Al atoms are in the coordination environment of Ge (2−4 Al neighbors) (see Figure 5, inset 1). The average number of Al octahedra surrounding Ge atoms in a nanotube is obtained as follows:

$$N_{Al} = \frac{6f(Ge_{co}) + 3f(Ge_{es})}{f(Ge_{co}) + f(Ge_{es})} \quad (2)$$

$$\frac{f(Ge_{co})}{f(Ge_{es})} = \frac{3 - N_{Al}}{N_{Al} - 6} \quad (3)$$

where $f(Ge_{co})$ and $f(Ge_{es})$ correspond to the fraction of Ge atoms in the core and the edge of nanotubes or nanotube fragments, respectively.

In our case, with $N_{Al} = 4.5$, eq 3 indicates $f(Ge_{co})/f(Ge_{es}) = 1$ or $f(Ge_{co}) = f(Ge_{es}) = 0.5$.

Within the imogolite structure, the Ge atoms are located in a circular fashion along the tube axis. Mathematically, an equal number of edge and core sites implies the presence of tubes with only four Ge rings. Assuming a circular precursor structure, this would indicate the presence of very short tube sections.

However, the SAXS data do not support this hypothesis, with regard to the structure of the precursor. At $t = 0$ days, the presence of a suspension of short nanotubes with an almost-constant diameter can be excluded from the absence of intensity oscillations (see Figure 3). Indeed,

(31) Masion, A.; Thomas, F.; Bottero, J.-Y. *J. Non-Cryst. Solids* **1994**, *171*(2), 191.

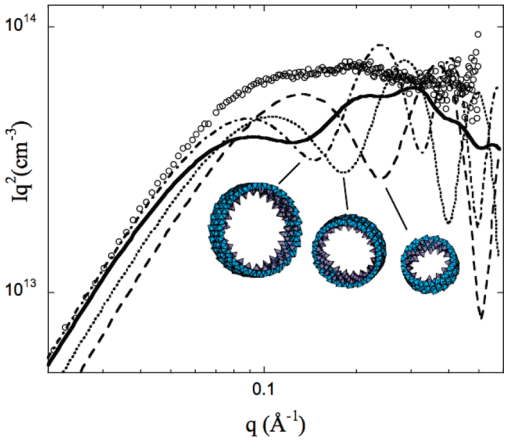

Figure 4. Iq^2 versus q plot for SAXS obtained for $t = 0$ days (open circle symbols, ○). The different lines are scattered intensities obtained for tubular-shaped precursors with 3 Ge rings of 15 (dashed line), 20 (dotted line), and 25 (dashed-dotted line) Ge atoms per ring. The solid line is the average scattering curve obtained for mixture of 22 tubular-shaped precursors with 4 rings of 15−36 Ge atoms per ring. (Light blue symbols represent Al octahedra, whereas purple-gray symbols represent Ge tetrahedra.)

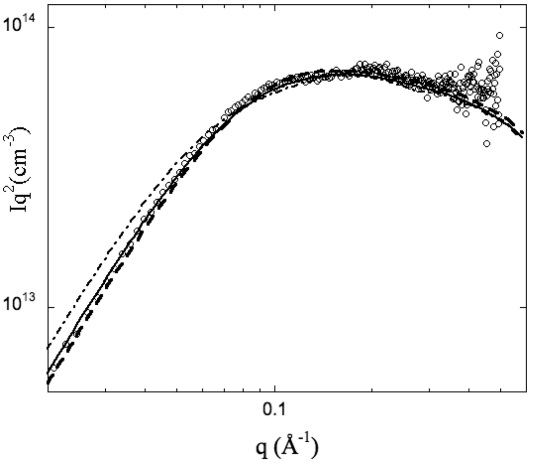

Figure 5. Iq^2 versus q plot for SAXS obtained for $t = 0$ days (open circle symbols, ○). The solid line is the averaged scattered intensities obtained for the precursor shapes of Table 3 containing 160 Al atoms per precursor. The dashed line and the dashed-dotted line are, respectively, average scattered intensities for similar shapes with 140 and 200 Al atoms per precursor.

because of their circular shape, such structures cause a marked oscillation of the scattered intensity. Also, a scattering signal similar to the $t = 0$ days curve cannot be obtained with a limited set of short tubes with varying diameter. Figure 4 shows the scattering curve computed for a mixture of 22 tubular precursors (each having equal weight in the simulation) of different diameter, ranging from 15 to 36 Ge atoms in the circumference. In parallel, the scattering curve of three isolated precursors are represented (15, 20, and 25 Ge atoms in the circumference). The oscillations, although considerably smoothed out at large q, because of the diameter polydispersity, are still clearly visible. Following this method, a complete smoothing of the signal would require a high level of polydispersity in ring diameter. However, this is not consistent with the scattering curves obtained with the samples after 2 and 5 days of

Table 3. Possible Models of Ge-Imogolite Precursor Nanotubes Containing ~160 Al Atoms[a]

	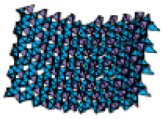	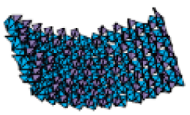	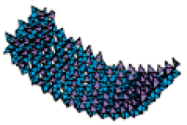	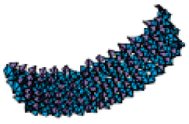	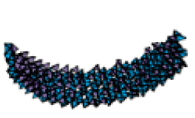	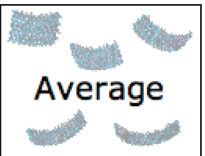
nb_{Al}	160	168	168	160	160	163
$R_{(Al/Ge)}$	2.10	2.13	2.13	2.13	2.13	2.12
N_{Al}	4.9	4.9	4.7	4.6	4.4	4.7
L(nm)	4.6	5.0	5.4	5.7	6.3	5.4

[a] For both models, the number of AL atoms (nb_{Al}), the Al/Ge ratio (R), the average number of Al neighbors per Ge atoms (N_{Al}), and the length (L, measured diagonally) are given. (Light blue symbols represent Al octahedra, whereas purple-gray symbols represent Ge tetrahedra.)

heating, which are characteristic of structures with almost-constant diameter (oscillations at the same q values).

Because circular structures can reasonably be excluded for the precursors, curved layers in the shape of roof tiles have been considered. Model structures have been built taking into account our experimental data concerning the coordination environment of Ge (4.5 Al neighbors), the proportion of edge and core sites $f(Ge_{co}) = f(Ge_{es}) = 0.5$, and the maximum size (~5 nm). Model structures with an increasing number of Al atoms (from 140 to 200) have been considered. Table 3 shows the different shapes that have been considered for the models containing 160 Al atoms. Figure 5 shows the scattering curves obtained for the models presented in Table 3 and similar models with an average number of Al atoms of 140 and 200. These curves fit the experimental data reasonably well.

For all models, an Al/Ge ratio of 2.13 is obtained, considering 20% Ge vacancies in the Ge layer. This value is close to the experimental value ($R_{exp} = 2.14$). When Ge vacancies are not introduced in the model precursors, not only is the Al/Ge ratio too low, compared to the experimental measurement, but the scattered intensity also is too strong, because of the increase in electronic density of the Ge layer (see Figure 6).

The best fit is obtained when the models have half the curvature of the final Ge-imogolite nanotube, to avoid intensity oscillatory features on the scattering signal. Indeed, the scattering of a precursor that has the final imogolite curvature displays marked intensity oscillations for $q > 0.1$ Å^{-1} (see Figure 6).

Of course, the models considered here are only a few possibilities for the structure of the precursors at $t = 0$ days. The actual precursor suspension consist most likely of several structures with variations in shape, size, curvature, and proportion of vacancies. It seems neither reasonable nor relevant to attempt to derive the precise composition of the suspension from the scattering data, since many combinations may fit the experimental curve. However, a mixture of our rooftile-shaped imogolite precursors appears to be a good candidate, since these

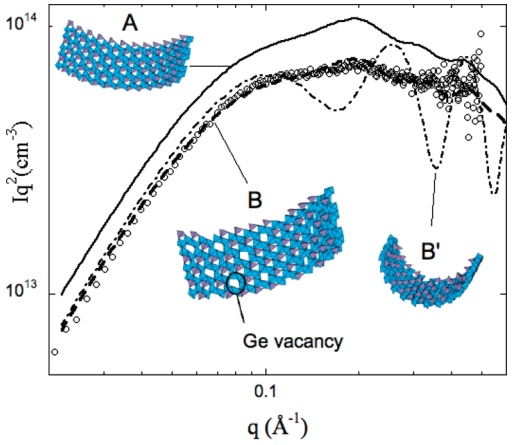

Figure 6. Iq^2 versus q plot for SAXS obtained for $t = 0$ days (open circle symbols, ○). The different lines are scattered intensities obtained for modification of the same precursor shape: Model A, without vacancies (solid line); model B, same as Model A, but with vacancies (dashed line); model B′, same as Model B, but with vacancies and the curvature of the final nanotube (dashed-dotted line). (Light blue symbols represent Al octahedra, whereas purple-gray sybmols represent Ge tetrahedra.)

models are based on the experimental data of three independent techniques, viz, EXAFS, NMR, and SAXS.

From the Precursors to the Nanoring/Nanotube. As already suggested for the formation of Si-imogolite,[10] the atoms in tetrahedral coordination may be responsible for the curvature of the gibbsite layer. In our case, the curvature may be the consequence of shorter O−O distances in the Ge tetrahedron (~2.8 Å) than in the Al dioctahedral vacancy (~3.2 Å) (see Figure 7, inset 2). Thus, increasing the number of Ge sites results in a more-curved structure. This mechanism is supported by our present SAXS computations, showing that Ge vacancies are a requirement for less-curved structures. The maximum of curvature is reached when all vacant sites on the gibbsite layer are occupied by Ge tetraedra, thus facilitating the nanotube formation.

Ge-Imogolite Growth by Edge−Edge Aggregation of Short Nanotubes. After two days of growth, the coordination environment of Al and Ge, as determined by EXAFS

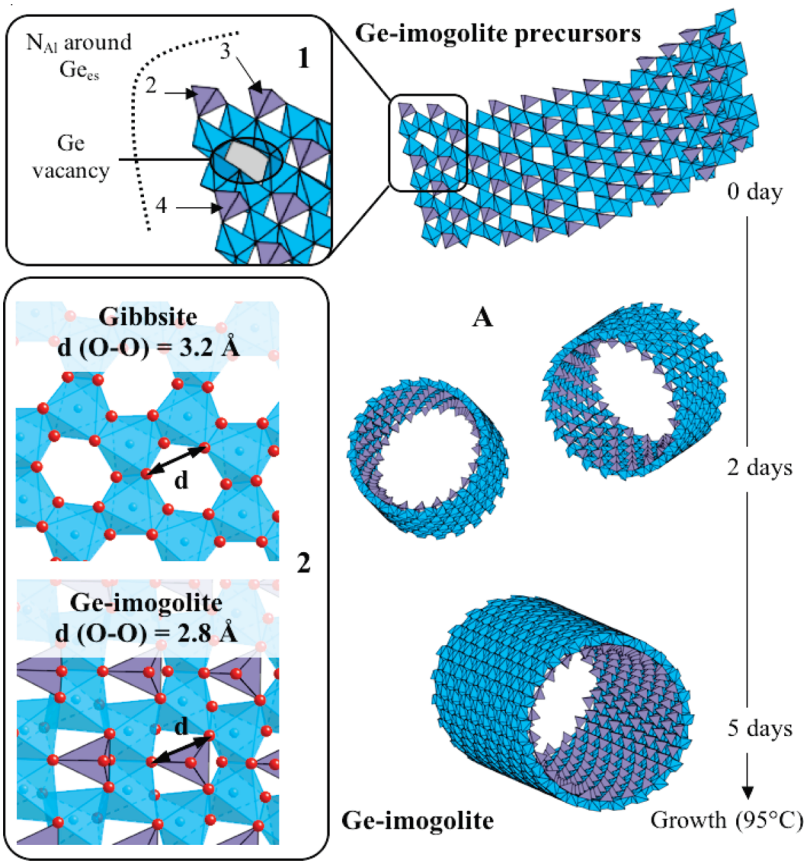

Figure 7. Proposed growth mechanisms of Ge-imogolite nanotubes. (Light blue symbols represent Al octahedra and purple-gray symbols represent Ge tetrahedra, whereas red spheres represent O atoms.)

and NMR, is characteristic of the final structure of Ge-imogolite, i.e., Al hydrolyzed and polymerized into a gibbsite layer configuration and Ge tetrahedra are linked to the gibbsite layer by 6 Al octahedra. At a larger scale, the first signs of nanotube formation are visible from 1 day of aging already, as evidenced by a modest onset of oscillations on the SAXS signal. The nanotube structure has clearly been observed for two and five days by SAXS. The two products exhibit a quasi-constant diameter. The difference between the two samples is an increase of the scattered intensity at low q. This increase without any shift of the oscillations is the signature of a growth in length of the nanotubes with a constant average diameter.

Between 2 and 5 days, the nanotubes grow from a suspension of nanotube sections and in the presence of a constant monomer fraction. This leads to the hypothesis that the final nanotubes are obtained from the assembly of already-formed shorter nanotubes or nanotube sections, rather than by the condensation of monomers on the nanotube edges. However, tube growth as a result of Ostwald ripening could lead to similar observations, in terms of dissolved monomer concentration and scattering volume fraction, and, therefore, may also occur.

Previous findings clearly demonstrated the tubular structure of the final product obtained under the present experimental conditions.[16] This is confirmed by the intensity oscillation at $q = 0.15$ Å^{-1} and $q = 0.32$ Å^{-1}, which is close to the theoretical values for a cylinder, i.e., 0.15 Å^{-1} and 0.34 Å^{-1}. The small discrepancy could be due to the defects in the semilocal structure that could arise during edge−edge assembly of tilelike nanotube sections. This will be further investigated in future work.

Conclusion

The growth mechanisms of Ge-imogolite have been investigated at the molecular and semilocal scales. The volume fraction of solids formed initially remains constant during the formation of the nanotubes: only the spatial organization of this solid phase evolves during the five days of reaction. A model structure for the precursors at $t = 0$ days consists of fragments of nanotubes of ~5 nm, with Ge vacancies and half the curvature of the final nanotube. The coordination environments of Al and Ge within the precursors show marked similarities with the final product. The final tubular structure is thought to be the result of an edge−edge assembly of shorter nanotube sections.

Acknowledgment. The authors would like to thank the iCEINT (international Center for the Environmental Implications of Nanotechnology) for providing and funding the collaborative framework concerning imogolite research.